Multiple Equilibria of the Global Thermohaline Circulation

JOCHEM MAROTZKE AND JÜRGEN WILLEBRAND

Institut für Meereskunde, Kiel, Federal Republic of Germany

(Manuscript received 10 August 1990, in final form 7 December 1990)

ABSTRACT

A general circulation model with a highly idealized geometry is used to investigate which fundamentally different equilibria of the global thermohaline circulation may exist. The model comprises two identical basins representing the Atlantic and Pacific oceans, which are connected by a circumpolar channel in the south. The model circulation is driven, in addition to wind forcing, by restoring the sea surface temperature to prescribed values and specified freshwater fluxes in the surface salinity budget (mixed boundary conditions). The boundary conditions are symmetric with respect to the equator and identical for both oceans.

Four fundamentally different, stable steady states are found under the same set of boundary conditions. Two of the equilibria show both oceans in the same state, with high-latitude deep-water formation occuring either in both northern or in both southern oceans, respectively. Two additional equilibria exist in which the thermohaline circulations of the basins differ fundamentally from each other: one ocean forms deep water at northern high latitudes, while the other has a much weaker circulation with sinking in the Southern Hemisphere. One of these equilibria qualitatively corresponds to today's global thermohaline circulation pattern (conveyor belt).

It is demonstrated that a transition from one equilibrium to another can be accomplished by relatively small differences in the freshwater fluxes. The preference and sensitivity of the steady states depends critically on the freshwater forcing applied.

1. Introduction

The thermohaline component of the ocean circulation that is forced by temperature and salinity differences between low and high latitudes plays a crucial role for climatic change on decadal and longer time scales. The thermohaline circulation provides the dominant transport of heat in the ocean (Bryan 1962; Hall and Bryden 1982) and has a large influence on the distribution of surface temperature and hence on the interaction between ocean and atmosphere. A striking feature of the global circulation system is the pronounced asymmetry between the Atlantic and Pacific oceans. The northern North Atlantic forms North Atlantic Deep Water (NADW) at a rate of about 15–20 Sv (Sv $\equiv 10^6$ m^3 s^{-1}) (Gordon 1986), whereas no corresponding water mass formation occurs in the North Pacific. Surface salinities in the North Pacific are so low that even water cooled down to the freezing point cannot sink to greater depths (Warren 1983). Consequently, abyssal water in the North Pacific is the oldest in the World Ocean as can be determined, e.g., from radiocarbon age measurements (Östlund and Stuiver 1980; Broecker and Peng 1982).

A gross sketch of the global meridional circulation has been developed by Gordon (1986): deep water is formed in the North Atlantic, moves southward across the equator and into the Indian and Pacific oceans, where it upwells and ultimately returns into the North Atlantic as thermocline water (the "conveyor belt"). While it is not completely clear to what extent the return flow of thermocline water occurs due to transport through the Indian Ocean and around Cape of Good Hope, as opposed to the Drake Passage, the important point is that, on annual average, warm near-surface water crosses the equator northward in the Atlantic, causing a cross-equatorial heat transport that is estimated to lie between 0.5 and 1.0 PW (e.g., Wunsch 1984; Hsiung 1985; Isemer et al. 1989, 1 PW = 10^{15} W), with strong impact on especially the European climate.

The cause for this circulation pattern has been attributed to different freshwater budgets in the Atlantic and the Pacific (Warren 1983; Broecker 1987). The density of seawater in the areas capable of deep-water formation is controlled by its salinity. The observed higher salinities of the North Atlantic as compared with the North Pacific are maintained by the enhanced evaporation rate due to higher surface temperatures. These in turn are brought about by cross-equatorial heat transport in the Atlantic, which is due to thermocline water being imported to the North Atlantic and deep water being exported from it. The deep current again is driven by the formation of NADW, caused by high surface densities in the northern North Atlantic, which are due to the relatively high salinities. The sys-

Corresponding author address: Dr. Jurgen Willebrand, Institut für Meereskunde, Dusternbrooker Weg 20, 23 Kiel, Federal Republic of Germany.

tem thus provides itself with the high North Atlantic salinities necessary to form NADW. Looking for the causes, one is faced with a "classic chicken and egg situation" (Broecker 1987), which is a typical characteristic of positive feedback mechanisms.

There is ample evidence from paleoclimatic records that the deep circulation of the World Ocean varied considerably in the past (e.g., Brass et al. 1982; Broecker et al. 1985; Boyle and Keigwin 1987; Duplessy et al. 1988). Broecker (1987) emphasizes that one of the main lessons to be learned from paleoclimatic records is the possibility of very rapid climate changes, like the onset and cessation of the Younger Dryas Event. Broecker et al. (1985) speculate that these changes reflect transitions between two quasi-stable equilibrium states of the oceanic circulation. They propose that during the glaciation, the Atlantic and Pacific interchanged their roles, e.g., the Pacific formed northern deep water and the Atlantic did not.

The different coupling of the temperature and salinity fields to the atmosphere is a crucial ingredient of all theoretical models that attempt to explain the existence of multiple stable equilibrium states of the ocean circulation. Because the surface heat flux strongly depends on the sea surface temperature (SST), SST anomalies are rapidly removed by enhanced heat gain or loss [the typical time scale of SST anomalies with spatial scales of o(1000) km is a few months]. The surface salinity, however, has negligible influence on evaporation and precipitation rates, and consequently surface salinity anomalies can persist on much longer time scales.

According to the different atmospheric couplings, boundary conditions on temperature and salinity in ocean models should be quite different. For temperature, a Newtonian condition specifying the heat flux as proportional to the difference between SST and a prescribed apparent atmospheric temperature (Haney 1971) appears to be a reasonable approximation. Note that this is nearly equivalent to a prescription of SST, as advective time scales are generally much longer than the time scale of the Newtonian condition. For salinity, however, there is no physical basis for an equivalent Newtonian condition, and a prescription of evaporation minus precipitation ($E - P$) independent of surface salinity seems much more justified. Evaporation is, of course, strongly dependent on SST, but for a more detailed prescription of ($E - P$) an explicit atmospheric model is needed.

Based on different boundary conditions for temperature and salinity ("mixed boundary conditions"), several models have shown multiple equilibria under identical forcing. Stommel (1961) constructed a simple box model where the transport between polar and equatorial box was proportional to their density difference. This model has two stable solutions, with opposite flow directions, provided that the time scales by which temperature and salinity are restored to prescribed surface values are sufficiently distinct. Rooth (1982) investigated the stability of a three-box model comprising one equatorial and two polar boxes. He suggested that a symmetric solution would become unstable and develop into a single pole-to-pole cell under sustained symmetric forcing. Welander (1986) showed that a similar model has four stable equilibria, two symmetric (both hemispheres identical) and two antisymmetric (both hemispheres in opposite modes). Walin (1985) discussed an advective feedback mechanism involving freshwater transport through the Bering Strait that could lead to an asymmetric circulation.

In a GCM with wind and thermohaline forcing symmetric to the equator, Bryan (1986) found that the symmetric solution was indeed unstable to a finite-amplitude perturbation. An instability developed that eventually produced a single pole-to-pole cell, as suggested by Rooth (1982). In a two-dimensional model by Marotzke et al. (1988) a similar transition was induced by an infinitesimal perturbation. Manabe and Stouffer (1988) found two stable steady states in a coupled ocean–atmosphere model, one state with a warm and salty northern North Atlantic and one with a cold and fresh one. The solutions did not differ very much in the Pacific, and the net precipitation–evaporation rates were very similar in the two cases. Maier-Reimer and Mikolajewicz (1989) obtained two analogous steady states with their global ocean model.

Whereas, under appropriate boundary conditions, the existence of multiple equilibria of the thermohaline circulation is now well established, the full range of possible equilibria of the global circulation has not yet been explored. Furthermore, the stability of the steady states has not been investigated systematically. To address those questions, we have performed experiments with a three-dimensional numerical circulation model with an idealized geometrical configuration. The model is intended to simulate the principal aspects of the global conveyor belt, in order to help understanding some of the physical mechanisms that set up the global thermohaline circulation; this may be important for changing the large-scale patterns.

The paper is organized as follows. In section 2, the numerical model, which is based on the code provided by M. Cox, is described, and the choices for atmospheric forcing and parametrization of subgrid-scale processes are briefly discussed. In section 3, various equilibrium solutions that are obtained under identical forcing are presented. In section 4 the sensitivity of the equilibrium solutions to perturbations in the freshwater fluxes is investigated; the results are summarized and discussed in section 5.

2. Model description and spinup

We use a "global" general circulation model (GCM) with a highly idealized geometry, which is depicted in Fig. 1. Since we are interested in the principal question

of which fundamentally different patterns of the global thermohaline circulation may possibly be achieved, we only preserve the major geometrical features of the World Ocean. The possible role of the Indian Ocean in the global deep circulation is ignored, and the model consists of two ocean basins, which in the south are connected by a circumpolar channel, reflecting the fact that the oceans are strongly coupled in the south and only very weakly in the north.

The Antarctic Circumpolar Current (ACC) introduces a fundamental asymmetry between Northern and Southern hemispheres. Besides, symmetry is maintained as far as possible: the basins have equal width of 60° longitude and extend from 64°S to 64°N, with a constant depth of 4500 m. To be definite, we henceforth refer to the basins as Pacific and Atlantic. It should always be kept in mind, however, that the two oceans are completely interchangeable in the model. In the channel region, periodic boundary conditions are imposed at the zonal boundaries. The width of the channel is specified somewhat arbitrarily to 16° latitude, providing for three meridional velocity grid points.

The model used is the GFDL primitive equation GCM, based on the method described by Bryan (1969), in the version documented and distributed by Cox (1984). With very few exceptions—which are listed below—the standard model was used, and for any further information the reader is referred to the above references.

The horizontal resolution is very coarse, 3.75° in longitude and 4° in latitude. There are 15 levels in the vertical, with resolution varying from 50 m near the surface to 500 m near the bottom. We neglect the non-

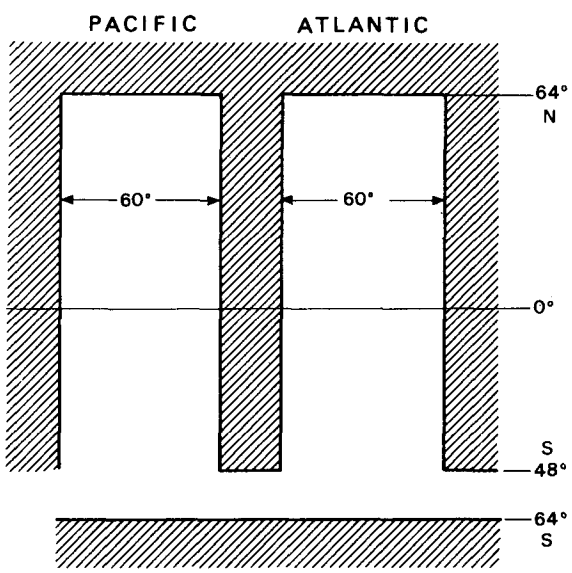

FIG. 1. Model domain of the global GFDL model.

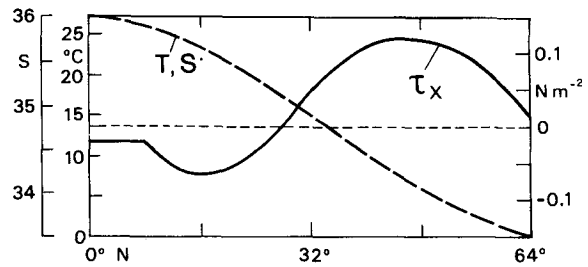

FIG. 2. Forcing fields of the model, as functions of latitude. Solid curve: zonal (eastward) wind stress τ_x in N m^{-2}, dashed curve: apparent atmospheric temperature T_a in degrees celsius and restoring salinity field S_a in psu. The forcing fields are symmetric about the equator and identical in both basins, so they are only shown for one hemisphere.

linear terms in the equations of motion since the Rossby number is only of order 0.01, even on grid-size length scale. As a consequence of the linear momentum balance and flat bottom, the vertically integrated transport depends only on the wind, i.e., there is no influence of the thermohaline circulation on the barotropic transport. The occurrence of unstable density stratification is handled by a convective adjustment scheme that guarantees complete removal of static instability. For a detailed discussion and comparison with the standard GFDL convective adjustment scheme see Marotzke (1991).

The bottom and the lateral walls are assumed insulating (zero heat and salt flux), at the lateral walls a "no slip" condition ($\mathbf{u} = 0$) is applied, at the bottom a "free slip" condition ($\partial_z \mathbf{u} = 0$) where $\mathbf{u} = (u, v)$ is the horizontal velocity. Wind stress is purely zonal and prescribed as a simple function of latitude only, reflecting the major features of the observed distribution (Fig. 2). It is symmetric about the equator and identical in both basins.

Although the choice of mixing coefficients is somewhat arbitrary, there are some guidelines. Bryan et al. (1975) report that a spatial computational mode is excited if the grid does not resolve the viscous western boundary layer. This means that, for a given resolution, the horizontal viscosity must be large enough to produce a boundary current of at least one gridpoint width. Bryan (1987) showed that thermocline depth, meridional overturning strength, and thus meridional heat transport increase with vertical diffusivity of heat and salt (i.e., the intensity of diabatic processes). Our values for the mixing coefficients are standard for coarse-resolution models. In close accordance to Bryan (1986, 1987), 2.5×10^5 m^2 s^{-1} and 10^{-4} m^2 s^{-1} for the horizontal and vertical viscosity, respectively, and 10^3 m^2 s^{-1} and 0.5×10^{-4} m^2 s^{-1} for the horizontal and vertical diffusivity, respectively, were chosen. The latter value is in the middle of the range explored by F. Bryan and used as his standard. These values are kept constant in all subsequent experiments.

The technique of asynchronous integration is applied, i.e., using different time steps in the heat/salt

and momentum/vorticity equations. As Bryan (1984) shows, this leaves the equilibrium solution unchanged but slows down internal gravity waves and external Rossby waves. Internal Rossby waves, which accomplish the adjustment of the density field to changes in the forcing (e.g., changes in the deep-water formation rate), are hardly affected since their wavelengths are large compared to the internal radius of deformation. Since we are mainly interested in processes of decadal and longer time scales, improper representation of the fast waves seems tolerable. Asynchronous integration thus makes an integration over thousands of oceanic years possible, while properly representing the processes of primary interest. The time step was two hours for the momentum equations and one day for temperature and salinity in all levels. In some experiments a time step of five days was possible for T and S.

To properly represent the physical processes that control the zonal transport of the ACC one would have to include bottom topography and the form drag induced by mesoscale eddies (Nowlin and Klinck 1986; Wolff and Olbers 1989). With a flat bottom and coarse resolution, a model would overestimate the ACC transport unless unrealistically high coefficients for the horizontal viscosity were used (Hidaka's dilemma). A scale analysis taking the no-slip boundary conditions into account (Marotzke 1990) and an idealized World Ocean model of a design similar to ours (Mead 1988) lead one to expect a model ACC transport of 200–400 Sv. In order to avoid any additional complications we decided to specify the ACC transport to a fixed value of 200 Sv. This is still too strong compared to the results from direct measurements (Whitworth and Peterson 1985) or inverse models (Olbers and Wenzel 1989), both giving about 125 Sv, but closer to the range of the estimates mentioned above. It should be kept in mind that the purpose of including the ACC in this study is to provide for a connection between the two ocean basins, in order to achieve an effective exchange of water mass properties.

The oceanic heat gain H_T at the surface is given as a Newtonian cooling law:

$$H_T = c\rho_0 D\lambda(T_a - T_S) \qquad (1)$$

where c is specific heat, D the depth of the top layer, λ^{-1} a time constant, and T_S surface temperature; T_a is a prescribed apparent atmospheric temperature (Haney 1971). Equation (1) means that the SST is restored to the prescirbed values T_a, with a time constant λ^{-1} chosen as 30 days. Here T_a is identical in the two basins and symmetric about the equator, and follows a cosine law in latitude with a difference of 27°C between high and low latitudes (Fig. 2), which resembles the observed, zonally averaged values (see Bryan 1987). It should be noted that restoring the SST with such a short time constant in practice very nearly means that we prescribe the SST since the advective time scales are generally much larger, except perhaps in the western boundary current.

For the surface salinity two different boundary conditions are used. In a spinup experiment the model is started from a state of rest, applying Newton-type boundary conditions on sea surface salinity with a time constant of 30 days, i.e., the same as for the surface temperature. This means to impose a surface freshwater flux $E - P$ of

$$E - P = \frac{D}{S_0}\lambda(S_a - S). \qquad (2)$$

Here S_a is analogous to the apparent atmospheric temperature T_a of Eq. (1), and S_0 is approximated as a constant reference salinity of 35 psu. Also S_a is identical in the two basins and symmetric about the equator and follows a cosine law in latitude with amplitude 2.5 psu (Fig. 2). A more realistic distribution for S_a would have to include a salinity minimum in the intertropical convergence zone. For the subsequent experiments only the equator-to-pole salinity contrast is relevant, and in our idealized model we have chosen maximum simplicity rather than maximum realism. The consequence of the boundary condition (2) is again to very nearly fix the surface values. In the experiments following the spinup, the surface freshwater fluxes are specified (mixed boundary conditions); the choice of $E - P$ is described below.

The spinup run is started from a state of rest with surface wind stress and restoring surface temperatures and salinities as depicted in Fig. 2. The model is integrated for 4816 years when a quasi-steady state has been reached (basin-averaged heat uptake less than 10^{-3} W m^{-2}). This spinup not only serves as initial state for most subsequent experiments but has some interesting aspects in itself.

Figures 3a and 3b show the salinity field, averaged zonally over both basins, and the streamfunction of the meridional mass transport, taken as the sum of both basins. While the zonally averaged temperature and salinity fields are nearly symmetric about the equator (Fig. 3a), the thermohaline circulation is highly asymmetric (Fig. 3b). Sinking at high northern latitudes occurs at a rate of 12 Sv in each basin whereas a hemispherewide overturning cell is absent in the south. Consequently, heat transport (not shown) is weak in the Southern Hemisphere; it is accomplished by diffusion in the ACC and by the wind-driven cell at low latitudes. The cross-equatorial heat transport amounts to 0.37 PW for both basins combined. The seeming discrepancy between T/S symmetry and overturning asymmetry also occurs in Cox's (1989) idealized World Ocean model; the thermohaline circulation (Fig. 3b) is similiar in structure to Mead's (1988) 2°-resolution model. To reconcile Figs. 3a and 3b it is necessary to consider the ACC dynamics more closely.

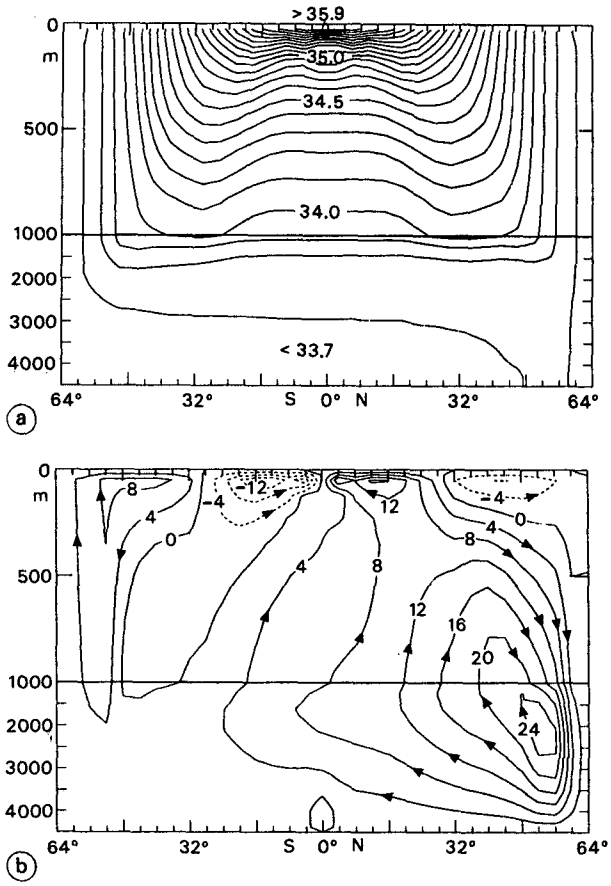

FIG. 3. Spinup steady state. (a) Zonally averaged salinity in psu and (b) meridional streamfunction in 10^6 m^3 s^{-1}, both basins combined.

Gill and Bryan (1971) found that in a single-hemisphere model including the ACC, the wind-driven cell associated with the westerlies extends to much greater depths than without a channel; in Fig. 3b the 4 Sv line reaches down to 2000-m depth in the ACC, compared to 150 m of the −4 Sv line in the Northern Hemisphere. Gill and Bryan (1971) attribute this to the fact that due to cyclic continuity no pressure difference between eastern and western boundaries can geostrophically balance the mean meridional flow, so the latter is greatly reduced. Part of it compensates the surface Ekman transport in the presence of zonal barriers; in the ACC complete compensation is achieved only at great depths. The poleward meridional flow north of the channel cannot proceed farther and must therefore sink and return equatorward at relatively shallow depths. The circulation in and south of the ACC is thus rather efficiently decoupled from the rest of the ocean (Gill and Bryan 1971; Bryan and Lewis 1979; Cox 1989). In accordance with reduced overturning strength, convective activity and thus heat loss is weaker in the Southern Ocean. The diminished rate of deep-water formation in the south allows the northern deep water to penetrate southward across the equator.

Figure 4 shows the $E - P$ rates $H_S(\lambda, \phi)$ diagnosed from the spinup. We identify regions of freshwater loss in low latitudes and freshwater gain over the western boundary currents in both hemispheres. Both can be understood from the Newtonian boundary conditions and the structure of the restoring salinity field. Equatorial surface waters are forced toward high salinities while the water advected poleward in the western boundary current receives freshwater to lower its salinity. The latter is highly unrealistic since the poleward advection should be accompanied by strong latent heat loss leading to a maximum in $E - P$ rather than a minimum.

A second region of high freshwater uptake are the northern high latitudes where the strong meridional transports of heat and freshwater lead to heat loss and freshwater gain, again due to the Newtonian boundary conditions. The zonal average of $H_S(\lambda, \phi)$, as diagnosed from the spinup, is shown as the dashed line in Fig. 5. The Northern Hemisphere received more freshwater than the Southern Hemisphere, which is associated with the northward salinity transport across the equator, due to the asymmetric meridional overturning. Using the $E - P$ fluxes from the spinup in the experiments with mixed boundary conditions thus introduces a bias, which amounts to about 0.1 Sv of southward freshwater transport across the equator, in each basin. It is because of this bias that in most experiments described below, the freshwater fluxes $H_S(\lambda, \phi)$ are not applied.

The solid line in Fig. 5 shows the freshwater fluxes $H(\phi)$ that were used in most runs with mixed boundary conditions. Here $H(\phi)$ is zonally invariant and sym-

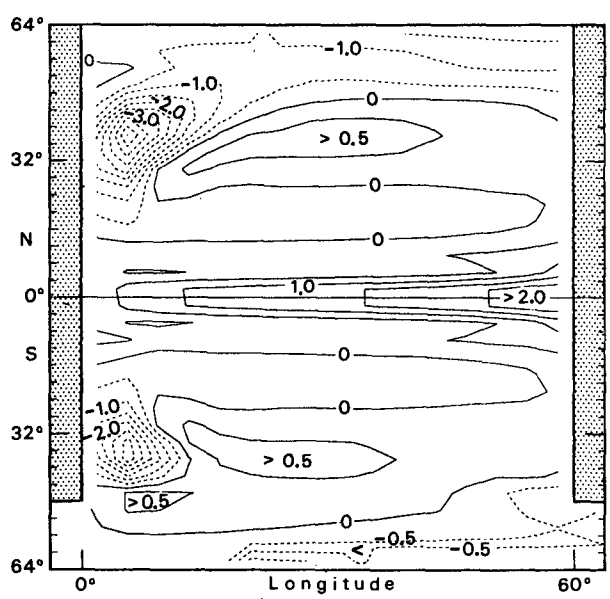

FIG. 4. Surface freshwater fluxes ($E - P$) in meters per year, diagnosed from the spinup. The field displayed is referred to as $H_S(\lambda, \phi)$ and is identical in both oceans.

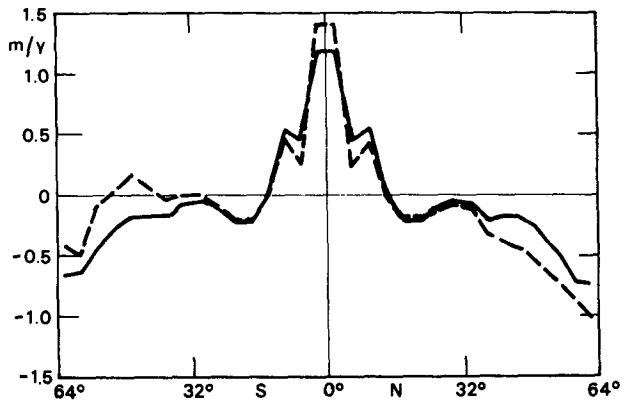

FIG. 5. Surface freshwater fluxes ($E - P$) in meters per year. Solid line: $H(\phi)$, i.e., $E - P$ is symmetric about the equator and zonally invariant. Dashed line: zonal average of $H_S(\lambda, \phi)$, diagnosed from the spinup (see Fig. 4).

metric about the equator, apart from a small reduction over the ACC, which accounts for the larger area in the channel region as compared to the same latitudes in the Northern Hemisphere. As a consequence, the steady-state meridional freshwater transport is zero at the equator since freshwater gain and loss exactly balance over each hemisphere. The field $H(\phi)$ was obtained by running a spinup in a manner similar to the one described above but for one hemisphere of one ocean basin only. From the steady state the freshwater fluxes necessary to maintain the surface salinities were diagnosed and averaged zonally. For further details, see Marotzke (1990). Note from Fig. 5 that the differences between $H(\phi)$ (solid line) and the zonal mean of $H_S(\lambda, \phi)$ (dashed line) are clearly visible but not dramatic.

3. Equilibrium states with mixed boundary conditions

a. Experiment I

The experiments that we performed to obtain multiple steady states under mixed boundary conditions are listed in Table 1. In experiment I the global spinup was taken as initial state, and mixed boundary conditions with freshwater fluxes $h(\phi)$ (Fig. 5) were applied. The model was integrated for 1643 years when it was apparent that further integration was unlikely to bring any substantial change. We have not used formal criterion for the definition of equilibrium states, but have required that the basin-averaged surface heat flux was below $O(0.1)$ W m^{-2}. The final state is termed equilibrium 1 ("northern sinking," see Table 1) and is displayed in Fig. 6, showing meridional volume transport, zonally averaged salinity, and meridional heat transport. Both basins are identical, so only zonal integrals over both oceans are displayed.

Comparing Fig. 6 to the spinup (Fig. 3) exhibits major differences, although sinking still takes place in both northern oceans. The strength of the meridional overturning has increased by 50%, maximum is now 18 Sv in each basin compared to 12 Sv for the spinup. Associated is a clearly asymmetric salinity field; at shallow depths northern high-latitude salinities are abougt 0.5 psu higher than their southern counterparts. Meridional heat transport (Fig. 6c) is very small south of 15°S and directed northward elsewhere, each basin having a cross-equatorial transport of 0.3 PW and a maximum of 0.7 PW, at 12°N. The stronger northward heat transport as compared to the spinup is a consequence of the more vigorous overturning.

The final state of experiment I was obtained by applying the symmetric $E - P$ field $H(\phi)$ to an initial state defined by the spinup, without introducing any

TABLE 1. Experiments leading to different steady states under mixed boundary conditions. δ is an $(E - P)$ anomaly of 0.18 m yr^{-1}, applied north of 44°N. A positive anomaly means excess evaporation. A time step of one day was used throughout, except in experiment 1, final phase, where a time step of five days was applied.

Experiment	Initial state	Preparation phase		Final phase		Final state
		$E - P$	Duration	$E - P$	Duration	
I	Spinup	—	—	$H(\phi)$	1643 y	Equilibrium 1: northern sinking (Fig. 6)
II	Spinup	$H(\phi)$ N. Atl.: $H(\phi) + \delta$ N. Pac.: $H(\phi) - \delta$	493 y	$H(\phi)$	985 y	Equilibrium 2: conveyor belt (Fig. 7)
IIa		Same as expt. II but sign of δ reversed				Equilibrium 3: inverse conveyor belt
III	Spinup −0.5 psu $\phi > 44$°N	$H_S(\lambda, \phi)$	739 y	$H(\phi)$	1561 y	Equilibrium 4: southern sinking (Fig. 8)
IV	Spinup	—	—	$H_S(\lambda, \phi)$	329 y	Equilibrium 4a: southern sinking (not shown)
V	Spinup	$H_S(\lambda, \phi)$ N. Atl.: $H_S(\lambda, \phi) + \delta$ N. Pac.: $H_S(\lambda, \phi) - \delta$	821 y	$H_S(\lambda, \phi)$	1478 y	Equilibrium 2a: conveyor belt (Fig. 9)

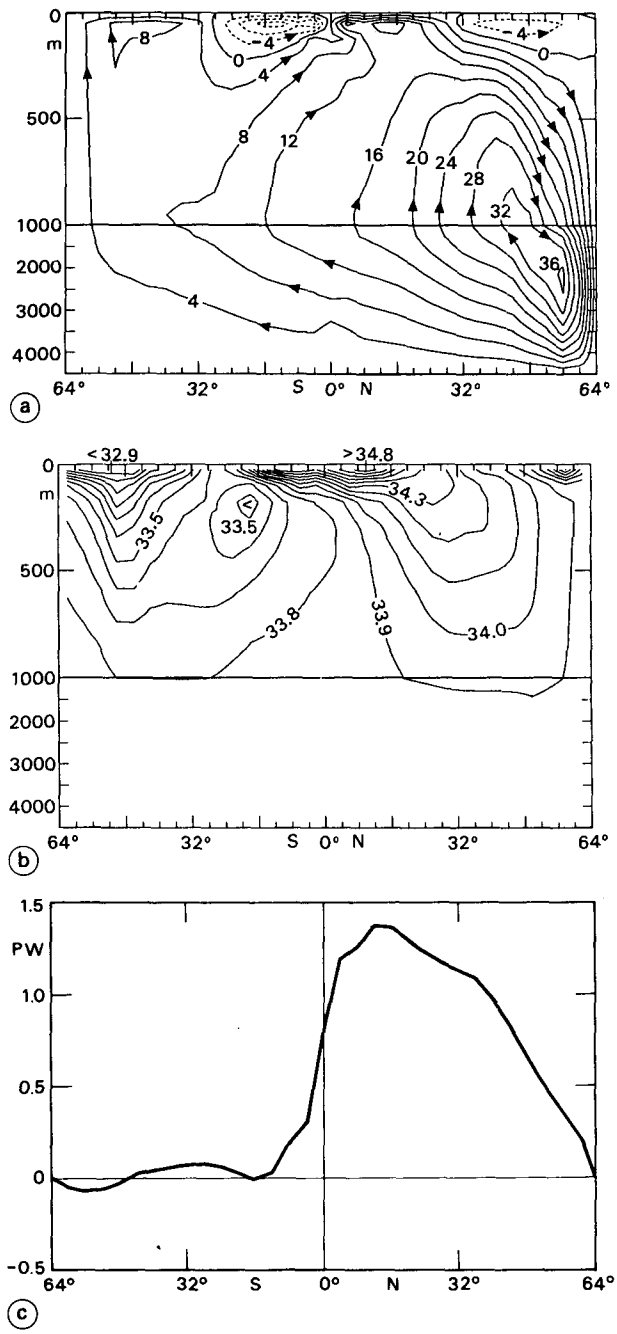

FIG. 6. Equilibrium 1: northern sinking. (a) Meridional streamfunction in 10^6 m^3 s^{-1} as the sum of both basins, (b) zonally averaged salinity in psu and (c) northward heat transport in PW for both basins combined.

bias toward northern deep-water formation. However, it could be argued (Mead 1988) that the asymmetric meridional circulation of the spinup introduces a bias by the initial northward salinity flux across the equator, favoring sinking in the north. This bias is removed in a further experiment in which the model is started from a state of rest and constant temperature/salinity fields, using the same mixed boundary conditions as in experiment I. Again equilibrium 1 results, showing that it is the asymmetric geometry of the model rather than asymmetries in the initial state that favors deep-water formation in the north.

b. *Experiment II*

We have attempted to find as many different equilibria of the model as possible, under the same boundary conditions. Different steady states can be achieved by choosing different initial conditions. The most obvious initial conditions, namely, the spinup or a state of rest, both lead to the equilibrium with sinking in both northern oceans. To achieve a final state different from equilibrium 1, we have to select particularly favorable initial conditions. Experience has shown that the most efficient way to construct such initial conditions is to introduce a temporary perturbation in $E - P$ that steers the solution toward a possible equilibrium state. After the model has adjusted to the perturbed freshwater fluxes, showing a flow pattern different from equilibrium 1, the perturbation in $E - P$ is switched off and the freshwater fluxes $H(\phi)$ from Fig. 5 are used again. If the structure of the circulation persists even after we have switched off the $E - P$ perturbation we have found another equilibrium with identical SST and freshwater fluxes.

In experiment II we aim at obtaining the conveyor belt, i.e., the state representing today's global thermohaline circulation, with NADW formation but no sinking in the North Pacific. To obtain an initial state favoring a conveyor-belt solution, an intermediate $E - P$ perturbation was chosen such that there is higher than normal evaporation over the Atlantic and lower evaporation over the Pacific. Consequently initial surface salinities should become higher in the North Atlantic and lower in the North Pacific.

The run starts from the spinup state; the freshwater fluxes $H(\phi)$ are perturbed by 0.18 m yr^{-1} north of 44°N so that there is excess evaporation over the Atlantic and excess precipitation over the Pacific. This amounts to an atmospheric water transport of 0.04 Sv from Atlantic to Pacific, which is at the lower end of the estimates given by Warren (1983). Due to the additional freshwater input, the Pacific overturning collapses within 30 years. Then sinking sets in north of the ACC region in the Pacific; simultaneously the Atlantic circulation is strengthened. This transition is completed within another 100 years. After 493 years of integration with the perturbed freshwater fluxes, the model has adjusted satisfactorily and the freshwater flux anomaly is switched off. With boundary conditions now identical to experiment I, the integration is continued for another 985 years when a new equilibrium, labeled equilibrium 2, has been reached (see Table 1).

Figure 7 shows that with boundary conditions identical for Atlantic and Pacific, the states in the two oceans

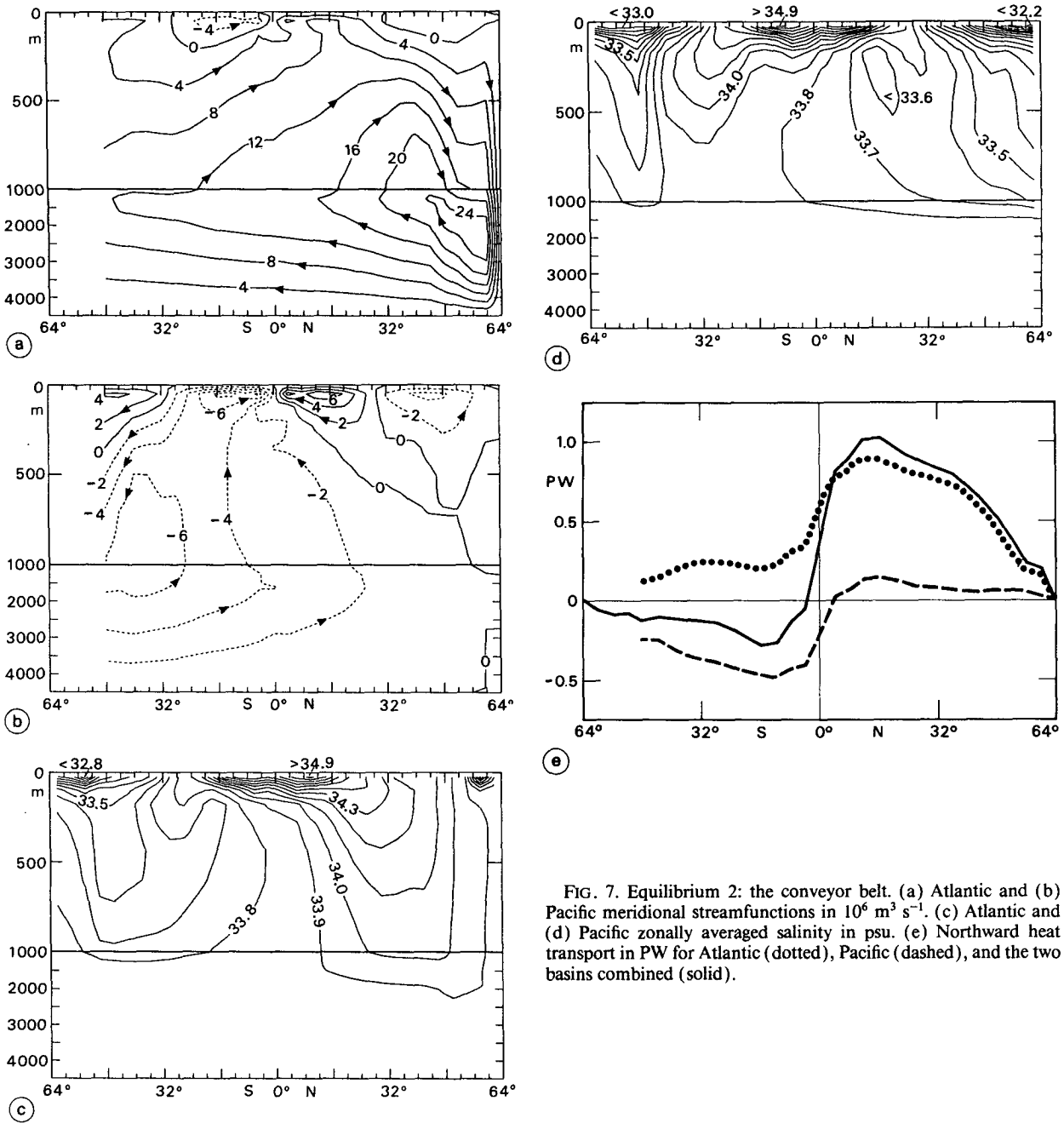

FIG. 7. Equilibrium 2: the conveyor belt. (a) Atlantic and (b) Pacific meridional streamfunctions in 10^6 m^3 s^{-1}. (c) Atlantic and (d) Pacific zonally averaged salinity in psu. (e) Northward heat transport in PW for Atlantic (dotted), Pacific (dashed), and the two basins combined (solid).

are completely different. Surface salinities are more than 1 psu higher in the North Atlantic than in the North Pacific. Associated NADW formation is at a rate of 25 Sv, twice the strength of the spinup overturning in one basin, and 25% stronger than in one basin of experiment 1. About 10 Sv of deep water are exported from the Atlantic and return as thermocline water (Fig. 7a). The Pacific, however, forms no deep water in the north, and has a generally much weaker thermohaline circulation, with a maximum of 7 Sv at about 40°S. Deep water is imported at a rate of 6 Sv (Fig. 7b). The global circulation thus qualitatively corresponds to the conveyor belt (Gordon 1986).

The circulation patterns are mirrored in the zonally averaged salinity fields: strong convective activity persists in the North Atlantic and determines the deep-ocean salinity. The deep North Pacific, however, is shielded from the surface by the low salinities at shallow depths. In the southern Hemisphere, warm and salty water originating from the subtropics extends to greater depths in the Pacific than in the Atlantic, where the combined wind-driven circulation in the ACC region

and thermohaline circulation north of it bring up very fresh water to 200-m depth at 16°S (Figs. 7c,d).

Meridional heat transports are displayed in Fig. 7e. Atlantic transport is 0.6 PW northward across the equator and has its maximum at 16°N with 0.9 PW. Again this means an increase of about 25%, compared to one basin of equilibrium 1 ("northern sinking"). Heat transport in the Pacific reaches less than half of the Atlantic's strength and is not as markedly asymmetric. Combined, the two oceans transport 0.35 PW northward across the equator.

The horizontal circulation patterns (not shown) are different in the different hemispheres, though not as dramatically as the meridional circulations. Generally the subtropical gyres are stronger in the basin halves where deep water is formed and weaker where no substantial sinking takes place. In order to compare the strength of the western boundary currents we consider transports between 0 and 1250 m in the two westernmost grid boxes since in a model with linear momentum balance and a flat bottom the vertically integrated transport solely depends on the wind-stress curl and hence is identical in both oceans. Poleward transports of 30 Sv and 11 Sv are found in the South Pacific and South Atlantic, respectively, and 22 Sv and 45 Sv in the North Pacific and North Atlantic, respectively. We conclude that the thermohaline component of the western boundary currents plays a major role, and that the horizonal gyres are stronger in the northern oceans than in the south, most likely due to the asymmetric geometry.

From the symmetry of our model it is clear that if the sign of the intermediate $(E - P)$ anomaly in experiment II is reversed, i.e., in the preparation phase there is excess evaporation over the Pacific and excess precipitation over the Atlantic, a state emerges in which the basins interchange their roles compared to the conveyor belt solution (experiment IIa, Table 1). This third equilibrium, termed "inverse conveyor belt," shows deep-water formation in the North Pacific and sinking in the South Atlantic, north of the ACC. Due to the symmetric geometry and forcing, the inverse conveyor belt is in every respect equivalent to the conveyor belt displayed in Fig. 7, only the Atlantic takes the Pacific's role and vice versa.

c. *Experiment III*

The clear preference of equilibrium 1 with freshwater fluxes $H(\phi)$ became evident in section 3a. As a consequence it required several attempts to find the starting point that finally would lead to the equilibrium forming no northern deep water at all. It is obvious that the aforementioned temporary perturbation in $E - P$ should produce enhanced precipitation over both northern oceans. The freshwater fluxes $H_S(\lambda, \phi)$ diagnosed from the global spinup have the desired property: there is net excess of precipitation over evaporation, averaged over the northern oceans (see Figs. 4 and 5), which in an equilibrium state corresponds to an export of freshwater from the Northern Hemisphere, at a rate of about 0.1 Sv in each basin.

Experiment III starts from the global spinup and applies the freshwater fluxes $H_S(\lambda, \phi)$ diagnosed from the spinup. In other words, the standard freshwater fluxes $H(\phi)$ are perturbed by $H_S(\lambda, \phi) - H(\phi)$. To speed up the desired breakdown of northern deep-water formation, an initial salinity anomaly of -0.5 psu was added to the top layer north of 44°N in both oceans. Sinking rapidly stops in the north and after 739 years an approximate steady state has been reached. The freshwater fluxes are now restored to the field $H(\phi)$, as for equilibria 1, 2, and 3. The integration is continued for another 1561 years.

In the resulting equilibrium 4 ("southern sinking," see Table 1) both oceans resemble the Pacific from the conveyor belt (equilibrium 2), especially in the Northern Hemisphere, but there are deviations in the south (Fig. 8). Salinities are higher in the Southern Ocean for the southern sinking (Fig. 8b), and overturning strength (Fig. 8a) shows an almost twofold increase compared to the Pacific from the conveyor belt (Fig. 7b). Meridional heat transports, however, are only slightly increased (compare Pacific heat transport in Fig. 7e with half of the total heat transport in Fig. 8c), since the main differences in overturning strength are at depths where no substantial vertical temperature variations occur.

4. Sensitivity of the equilibria to changes in freshwater fluxes

In section 3 we described how four different steady states of the global thermohaline circulation are obtained under identical boundary conditions. We now want to investigate how the equilibria react to changes in the freshwater fluxes. It is clear that a complete description of the stability of the equilibria cannot be given for a 3 D model, even for the idealized one employed here. One would have to vary the $E - P$ field systematically and perform a series of perturbation experiments for each set of freshwater fluxes. Since a typical experiment with the global model requires 10–20 hours CPU on a CRAY-XMP, some long-term runs even more, any systematic exploration of the phase space is infeasible. For this reason we concentrate on the sensitivity of the conveyor belt equilibrium which corresponds to today's global thermohaline circulation.

In the course of experiment II we conceptually introduced an intermediate atmospheric water vapor transport from the North Atlantic to the North Pacific. Now we want to investigate how the conveyor belt circulation (equilibrium 2, Table 1) reacts if an atmospheric water vapor transport of reversed sign is assumed, i.e., enhanced evaporation occurs over the North Pacific and enhanced precipitation over the

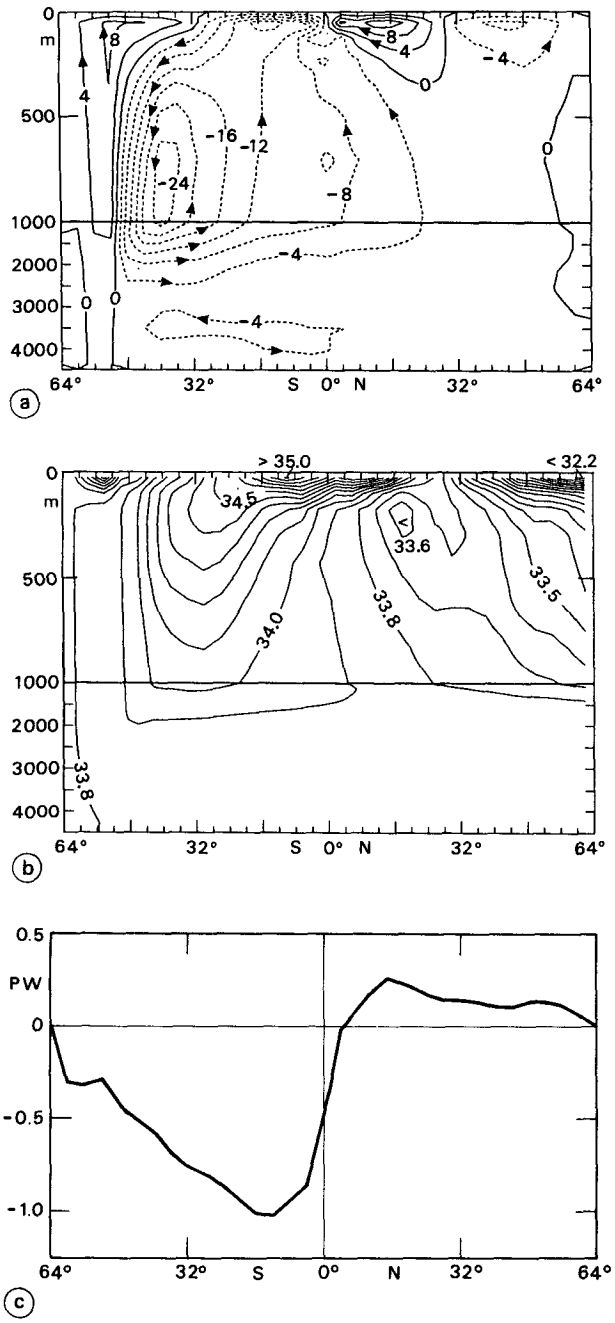

FIG. 8. Equilibrium 4: southern sinking. (a) Meridional streamfunction in 10^6 m^3 s^{-1} as the sum of both basins, (b) zonally averaged salinity in psu and (c) northward heat transport in PW for both basins combined.

North Atlantic (experiment S1, Table 2). We start from equilibrium 2, the conveyor belt, and change the ($E - P$) fluxes $H(\phi)$ by +0.18 m yr^{-1} in the North Pacific and −0.18 m yr^{-1} in the North Atlantic, again north of 44°N. Increased evaporation over the North Pacific initiates deep-water formation there whereas no qualitative change takes place in the North Atlantic. After 1478 years experiment S1 results in a circulation resembling equilibrium 1 (northern sinking). This is one more manifestation of the preference of the northern sinking equilibrium due to the asymmetries introduced by the geometry of the model. Note, however, that equilibrium 1 could only be reached exactly when the differences in freshwater fluxes between North Atlantic and North Pacific, which were maintained during all of experiment S1, were switched off again.

Experiment S2 (see Table 2) is designed analogous to S1 but the changes in the freshwater fluxes $H(\phi)$ are doubled in magnitude. That is, experiment S2 starts from equilibrium 2, the conveyor belt, and uses the $E - P$ field $H(\phi)$ changed by 0.36 m yr^{-1} excess evaporation over the Pacific and 0.36 m yr^{-1} excess precipitation over the Atlantic, both north of 44°N. The model is integrated for 657 years; the changed freshwater fluxes cause both oceans to change their behavior in regard to deep-water formation in the Northern Hemisphere: the model flips to a state with formation of "North Pacific Deep Water" but no NADW formation, a state resembling the inverse conveyor belt (Table 1). The cessation of NADW formation occurs within 25 years, whereas the buildup of "NPDW" formation takes about 100 years. This is the transition that Broecker et al. (1985) speculate may have taken place at the beginning of the ice age. We see that this complete reversal is dynamically possible and occurs very fast, compared to geological time scales. The implied atmospheric water vapor transport, however, which is about 0.08 Sv from the Pacific to the Atlantic, is so drastically different from today's that within the limits of our model it appears rather unlikely. It is not clear how the situation would be if SST and $E - P$ were allowed to vary, as a consequence of changes in the heat transport. Variations in the freshwater input could also be caused by changes in the tranpsorts through the Bering Strait (Walin 1985), or from changes in the runoff from glaciers, as assumed by Maier-Reimer and Mikolajewicz (1989).

In experiment I starting from the spinup and applying the freshwater fluxes $H(\phi)$, which are zonally invariant and symmetric about the equator, equilibrium 1 ("northern sinking," see Table 1) results if no perturbation is applied. In experiment S1 (Table 2) only the Pacific flips to a different state, i.e., it starts forming deep water in the north. The question to be addressed now is whether the preference of the northern sinking equilibrium persists if the freshwater fluxes change significantly. We will repeat some of the experiments described above but use the freshwater fluxes $H_S(\lambda, \phi)$ diagnosed from the global spinup, instead of the fluxes $H(\phi)$.

Experiment IV (see Table 1) starts from the spinup and uses the freshwater fluxes $H_S(\lambda, \phi)$ diagnosed from the spinup. This means that the spinup is an exact steady state even under mixed boundary conditions. However, the freshwater fluxes $H_S(\lambda, \phi)$ show no strong

TABLE 2. Sensitivity experiments for the conveyor-belt equilibria. Again δ is an $(E - P)$ anomaly of 0.18 m yr^{-1}, applied north of 44°N.

Expt.	Initial state	$E - P$	Duration	Final state
S1	Equilibrium 2: conveyor belt	$H(\phi)$ N. Atl.: $H(\phi) - \delta$ N. Pac.: $H(\phi) + \delta$	1478 yr	Northern sinking
S2	Equilibrium 2: conveyor belt	$H(\phi)$ N. Atl.: $H(\phi) - 2\delta$ N. Pac.: $H(\phi) + 2\delta$	657 yr	Inverse conveyor belt
S3	Equilibrium 2a: conveyor belt	$H_S(\lambda, \phi)$ N. Atl.: $H_S(\lambda, \phi) - \delta$ N. Pac.: $H_S(\lambda, \phi) + \delta$	329 yr	Southern sinking

excess precipitation over the Northern Hemisphere (see Figs. 4 and 5) that deep-water production there is severely inhibited. The following collapse of the circulation resembles the "halocline catastrophy" first observed by Bryan (1986), showing that the spinup equilibrium is unconditionally unstable with mixed boundary conditions, and after 329 years a state similar to equilibrium 4 has emerged. We term this steady state equilibrium 4a (Table 1). Comparison between experiments I and IV shows that $H_S(\lambda, \phi)$ introduces such a strong bias toward inhibiting deep-water formation in the north that it outweighs the one induced by the asymmetric geometry. Deep-water formation in the north is so severely inhibited that despite several attempts we did not succeed in obtaining a state resembling equilibrium 1 (northern sinking) with the $E - P$ field $H_S(\lambda, \phi)$.

While a northern sinking equilibrium with freshwater fluxes $H_S(\lambda, \phi)$ was not found, we did find the conveyor belt as a solution (experiment V, Table 1). The strategy was very similar to the one used in experiment II: starting from the spinup, the freshwater fluxes $H_S(\lambda, \phi)$ were perturbed by 0.18 m yr^{-1} north of 44°N, such that there was excess evaporation over the North Atlantic and excess precipitation over the North Pacific. With these fluxes the model was integrated for 821 years; then the perturbation was switched off. The integration was continued for another 1478 years, and by this time a steady state was reached, apart from a quasi-stationary oscillation with a period of roughly 30 years, which is associated with intermittent convective activity in the ACC region (see Marotzke 1990).

Figure 9 displays the most characteristic features of the final state, which we call equilibrium 2a. Surface salinities (not shown) vary over a much greater range than in equilibrium 2, and especially the northeastern parts are markedly depleted of salt, reflecting the very strong freshwater input there. The zonal salinity gradient results in a strengthening of the meridional overturning north of 48°N; for the other latitudes, the Atlantic circulation is weaker than in equilibrium 2 (Figs. 7a, 9a), whereas it is relatively more vigorous in the Pacific (Figs. 7b, 9b). As a consequence, Atlantic and total northward heat transports are reduced, and there is a combined transport of only 0.1 PW across the equator (not shown).

The two conveyor belts (equilibria 2 and 2a, Table 1) are qualitatively equivalent, although differences due to the different freshwater fluxes are clearly visible. We now want to investigate how the conveyor belt 2a, displayed in Fig. 9, reacts if the freshwater fluxes are changed analogously to experiment S1. Experiment S3

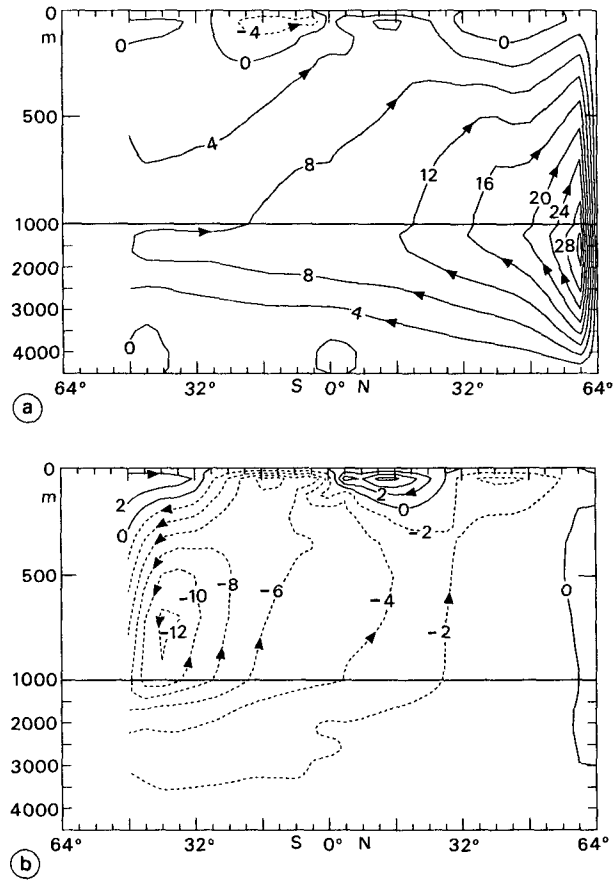

FIG. 9. Equilibrium 2a: the second version of the conveyor belt, obtained with the freshwater fluxes $H_S(\lambda, \phi)$ that were diagnosed from the spinup (see Fig. 4). (a) Atlantic and (b) Pacific meridional streamfunction in 10^6 m^3 s^{-1}.

(Table 2) starts from equilibrium 2a and uses $H_S(\lambda, \phi)$ as $E - P$ field, changed by $+0.18$ m yr^{-1} over the North Pacific and -0.18 m yr^{-1} over the North Atlantic, both north of 44°N. Now the North Pacific thermohaline circulation is essentially unchanged, whereas NADW formation ceases and sinking eventually occurs in the South Atlantic, north of the ACC. After 329 years experiment S3 leads to a state similar to equilibrium 4a, i.e., the second version of the southern sinking equilibrium (see Table 1).

Recalling what has been said about which steady states were preferred by the sets of freshwater fluxes, $H(\phi)$ and $H_S(\lambda, \phi)$, we see that when $E - P$ is changed by as much as in experiments S1 and S3, the conveyor belt circulation in both experiments shifted over to the respective "favored" equilibrium, northern sinking with $H(\phi)$ and southern sinking with $H_S(\lambda, \phi)$. The atmospheric water vapor transport of 0.04 Sv, implied by the perturbation, is not a small amount. However, we see from Fig. 5 that on zonal average the difference between the sets of freshwater fluxes, $H(\phi)$ and $H_S(\lambda, \phi)$ is a gradual one rather than qualitative, given the uncertainties in $(E - P)$ measurements. Thus with both sets of $E - P$ displayed in Fig. 5, today's global thermohaline circulation pattern can be realized, but the reaction to a modest perturbation in the water flux rates, as in experiments S1 and S3, will be dramatically different in the two cases.

Apart from the existence of multiple equilibria, the sensitivity of the model results to modest changes in freshwater fluxes is perhaps the most important result of this study. Mead (1988) performed experiments of a kind similar to ours. He used water fluxes that were zonally invariant and symmetric about the equator, but adapted the fields from Baumgartner and Reichel (1975), which have only half the amplitude of the distribution used here. In this case, excess precipitation of 0.25 m yr^{-1} over the Pacific did not produce the conveyor belt, but rather northern sinking circulation with weakened Pacific overturning. This is most likely due to the generally reduced salinity influence on the thermohaline circulation, visible for example in surface salinity contrasts which on zonal average are about 1.0 psu between high and low latitudes, compared to typically 2.0 psu in our experiments. We conclude that without a precise knowledge of the $E - P$ rates to be applied no reliable statement can be made about the most probable equilibrium solution of the global thermohaline circulation.

5. Discussion

In this paper we have identified qualitatively different equilibria of the global thermohaline circulation, using an ocean general circulation model for an idealized global domain with two identical ocean basins connected in the Southern Hemisphere. As in earlier studies, the crucial feature enabling multiple steady states is the different coupling of the temperature and salinity fields to the atmosphere. Whereas sea surface temperature is effectively prescribed, a flux condition for salinity at the ocean surface is employed (mixed boundary conditions). Thus the close coupling of SST anomalies to the surface heat flux and the independence of evaporation and precipitation of the surface salinity field are at least qualitatively accounted for.

Four fundamentally different steady-state solutions of our idealized global ocean model have been found for boundary conditions that are symmetric about the equator and identical in the two basins.

In equilibrium 1 (northern sinking) the circulation in both oceans is identical. Deep water is formed in both northern basins and is associated with a strong northward heat transport, while circulation and heat transport in the Southern Hemisphere are much weaker.

Equilibrium 2 (conveyor belt) most closely corresponds to the observed global thermohaline circulation pattern, with deep-water formation only in the North Atlantic but not in the North Pacific. As a consequence of the meridional flow, model heat transports are purely northward in the Atlantic and poleward but much weaker in the Pacific.

A further equilibrium state (inverse conveyor belt) is identical to equilibrium 2 except that the roles of Atlantic and Pacific are interchanged. It is interesting to note that a similar solution (high salinities in the North Pacific, low vaues in the North Atlantic) was obtained in the first experiment with a coupled ocean–atmosphere model and realistic geometry by Bryan et al. (1975). Our findings suggest that this was an accidental consequence of their choice of initial conditions, rather than any defect in the model.

The conveyor belt solutions demonstrate that even under identical forcing two oceans connected in the south may show completely different thermohaline flows. The different circulation and heat transport patterns are maintained while $E - P$ and very nearly also SST are forced to be identical in the two basins. In reality, the enhanced Atlantic heat transport warms surface water and leads to higher air temperature over the North Atlantic. Our results suggest that these higher temperatures are a consequence of the asymmetric thermohaline circulation, rather than being the fundamental cause for its maintenance as assumed by Warren (1983) and Broecker (1987). It is of course obvious that the dependence of evaporation on SST will act as a positive feedback to amplify the differences between both northern basins.

Equilibrium 4 (southern sinking) has again identical circulation patterns in both oceans, but deep water is formed in the southern Hemisphere north of the circumpolar current. Cross-equatorial heat transport is directed southward, its magnitude is somewhat reduced compared to equilibrium 1. Qualitatively, this equilibrium has been obtained by Maier-Reimer and Miko-

lajewicz (1989) and also in the coupled ocean–atmosphere model of Manabe and Stouffer (1988).

The results obtained in this study suggest that the circulation in each hemisphere can operate in two modes: 1) one mode with deep-water formation at high latitudes and associated strong poleward heat transport and 2) the other without deep-water formation and weak or equatorward heat transport. If all combinations of the two modes in the four basin halves were possible, there would be a total of 16 different steady states, which can actually be shown to exist in a box model comprising the Atlantic and the Pacific, with a connection in the Southern Ocean (Marotzke 1990). Therefore, the question arises whether the global GCM has any further equilibrium states. We have performed about 25 different experiments but did not find other steady states except those discussed above. While we cannot prove the nonexistence of further equilibrium states from any number of forward integrations in time, it is nevertheless interesting to speculate on the reasons for this negative result.

The four stable states that exist for the global GFDL model all are asymmetric with respect to the equator, both in the meridional circulation and in the salinity fields. All of the 12 remaining equilibria that are conceivable should show some symmetry at least in one basin, e.g., sinking in both high latitudes of one ocean or, recalling the lesson from the spinup, at least symmetric salinity fields. It appears that the presence of the ACC prevents a symmetric circulation with sinking in both high latitudes of a basin (see section 2, especially Fig. 3b). Resulting is the instability of the spinup under mixed boundary conditions because the asymmetric circulation rapidly destroys the symmetry in the salinity field as soon as surface salinities are no longer fixed. If, with this argument, we exclude all of the 16 box model equilibria with sinking in both high latitudes of one ocean, nine steady states would remain.

Equilibrium states symmetric to the equator could also exist if both hemispheres in one ocean did not exhibit sinking at high latitudes. The thermohaline circulation would be salinity dominated, i.e., sinking would take place at low latitudes where surface salinities are high. It has long been known (Stommel 1961; Welander 1986) that this inverse circulation exists in box models; it was also found in the two-dimensional model of Marotzke (1989).

It is conceivable that in the global GCM an equilibrium state would exist that shows sinking at low latitudes, at least in one basin. Marotzke (1989, 1990) has indeed shown that the inverse circulation exists as a quasi-steady state of a one-hemisphere GCM driven by purely thermohaline forcing. However, the inverse circulation has not been found in analogous experiments that included wind forcing. Apparently, the wind forcing induces such strong poleward salt transports that the very high meridional salinity differences necessary for the inverse circulation (about 8 psu) cannot build up. This argument would exclude five equilibrium states with equatorial sinking in at least one ocean, and only the four steady states remain that show no symmetry about the equator. Hence, our conclusion is that the wind forcing precludes, or at least reduces the likelihood of, any further equilibrium states.

Which of the different equilibrium states is favored depends very sensitively on the surface freshwater fluxes; relatively small variations in $(E - P)$ can change preference completely. While for the freshwater fluxes $H(\phi)$ the northern sinking solution was the preferred equilibrium, for the slightly different fluxes $H_S(\lambda, \phi)$ the southern sinking state emerged in most experiments. Transitions from one equilibrium to another are accomplished by $(E - P)$ differences between the two oceans corresponding to atmospheric water vapor transports well within the observed order of magnitude.

Our results have been obtained for a very idealized configuration, and cannot immediately be applied to the real ocean. The geometry of the world ocean and the actual atmospheric forcing are likely to have a significant influence on existence and preference of equilibrium states. For example, the different northward extent of Atlantic versus Pacific basins clearly is important for the amount of deep-water formation and hence could be crucial for determining which of the solutions is preferred. This could be particularly important for the question of whether an inverse conveyor belt solution is indeed possible. The role of the Indian Ocean for the global circulation pattern is less clear. It is possible that evaporation in the subtropical Indian Ocean could influence the salinity budget of conveyor belt solutions. However, so far all global-ocean models with realistic geometry and asymmetric forcing have obtained steady states that qualitatively correspond to one of the four stable equilibria listed above. In particular, we believe that the experiment by Bryan et al. (1975) indicates that an inverse conveyor belt solution can be found with realistic geometry. This suggests that although asymmetries in geometry and forcing probably have a major influence on the preference of steady states, our idealized model contains the basic mechanism responsible for the existence of multiple equilibria. Nevertheless, a more realistic model may not have all of the steady states found here, and equilibria may exist that could not be realized here.

The demonstrated sensitivity of the circulation patterns to the surface freshwater fluxes has important consequences for any attempt to realistically simulate the global thermohaline circulation and its changes. To properly predict which of the several stable modes of operation is actually obtained requires a better knowledge of the freshwater fluxes than is currently available. This deficiency also affects coupled ocean–atmosphere models where precipitation is most difficult to predict. A more accurate description of the global

hydrological cycle therefore is of fundamental importance for improved simulations of the global thermohaline circulation and its sensitivity to climatic change.

Acknowledgments. We are indebted to Michael Cox who provided the code for the circulation model used in this study. This is a contribution of the Sonderforschungsbereich "Warmwassershäre des Atlantiks," which is supported by the Deutsche Forschungsgemeinschaft.

REFERENCES

Baumgartner, A., and E. Reichel, 1975: *Die Weltwasserbilanz.* Oldenbourg, München, 179 pp.

Boyle, E. A., and L. Keigwin, 1987: North Atlantic thermohaline circulation during the past 20,000 years linked to high-latitude surface temperature. *Nature,* **330,** 35–40.

Brass, G. W., J. R. Southam and W. H. Peterson, 1982: Warm saline bottom water in the ancient ocean. *Nature,* **296,** 620–623.

Broecker, W. S. 1987: Unpleasant surprises in the greenhouse? *Nature,* **328,** 123–126.

——, and T. H. Peng, 1982: Tracers in the Sea. Lamont-Doherty Geological Observatory, Columbia University, 690 pp.

——, D. M. Peteet and D. Rind, 1985: Does the ocean–atmosphere system have more than one stable mode of operation? *Nature* **315,** 21–26.

Bryan, F., 1986: High-latitude salinity effects and interhemispheric thermohaline circulation. *Nature,* **323,** 301–304.

——, 1987: Parameter sensitivity of primitive equation ocean general circulation models. *J. Phys. Oceanogr.,* **17,** 970–985.

Bryan, K., 1962: Measurements of meridional heat transport by ocean currents. *J. Geophys. Res.,* **67,** 3403–3414.

——, 1969: A numerical method for the study of the circulation of the world ocean. *J. Comput. Phys.,* **3,** 347–376.

——, 1984: Accelerating the convergence to equilibrium of ocean-climate models. *J. Phys. Oceanogr.,* **14,** 666–673.

——, and L. J. Lewis, 1979: A water mass model of the world ocean. *J. Geophys. Res.,* **84,** 2503–2517.

——, S. Manabe and R. Pacanowski, 1975: A global ocean–atmosphere climate model. Part II: The oceanic circulation. *J. Phys. Oceanogr.,* **5,** 30–46.

Cox, M. D., 1984: A primitive equation, 3-dimensional model of the ocean. GFDL Ocean Group Tech. Rep. No 1, GFDL/Princeton University.

——, 1989: An idealized model of the world ocean. Part 1: The global-scale water masses. *J. Phys. Oceanogr.,* **19,** 1730–1752.

Duplessy, J. C., N. J. Shackleton, R. G. Fairbanks, L. Labeyrie, D. Oppo and N. Kallel, 1988: Deepwater source variations during the last climatic cycle and their impact on the global deepwater circulation. *Paleoceanogr.,* **3,** 343–360.

Gill, A. E., and K. Bryan, 1971: Effects of geometry on the circulation of a three-dimensional southern-hemisphere ocean model. *Deep-Sea Res.,* **18,** 685–721.

Gordon, A. L., 1986: Interocean exchange of thermocline water. *J. Geophys. Res.,* **91,** 5037–5046.

Hall, M. M., and H. L. Bryden, 1982: Direct estimates and mechanisms of ocean heat transport. *Deep-Sea Res.,* **29,** 339–359.

Haney, R. L., 1971: Surface thermal boundary condition for ocean circulation models. *J. Phys. Oceanogr.,* **1,** 241–248.

Hsiung, J., 1985: Estimates of global oceanic meridional heat transports. *J. Phys. Oceanogr.,* **15,** 1405–1413.

Isemer, H. J., J. Willebrand and L. Hasse, 1989: Fine adjustment of large scale air–sea energy flux parameterization by a direct estimate of ocean heat transport. *J. Climate,* **2,** 1173–1184.

Maier-Reimer, E., and U. Mikolajewicz, 1989: Experiments with an OGCM on the cause of the Younger Dryas. Report No. 39, Max-Planck-Institut für Meteorologie, Hamburg. Reprinted from: *Oceanography 1988* (Eds.: Ayala-Castanares, W. Wooster and A. Yanez-Arancibia), UNAM Press, Mexico D.F., 87–100.

Manabe, S., and R. J. Stouffer, 1988: Two stable equilibria of a coupled ocean-atmosphere model. *J. Climate,* **1,** 841–866.

Marotzke, J., 1989: Instabilities and multiple steady states of the thermohaline circulation. *Oceanic Circulation Models: Combining Data and Dynamics,* D. L. T. Anderson and J. Willebrand, Eds., Kluwer, 501–511.

——, 1990: Instabilities and multiple equilibria of the thermohaline circulation. Ph.D. thesis. Ber. Inst. Meeresk. Kiel, 194, 126 pp.

——, 1991: Influence of convective adjustment on the stability of the thermohaline circulation. *J. Phys. Oceanogr.,* in press.

——, P. Welander and J. Willebrand, 1988: Instability and multiple steady states in a meridional-plane model of the thermohaline circulation. *Tellus,* **40A,** 162–172.

Mead, C. T., 1988: Asymmetries of the oceanic thermohaline circulation and meridional heat transport. Ph.D. thesis, University of Southampton, 253 pp.

Nowlin, W. D., Jr., and J. M. Klinck, 1986. The physics of the Antarctic Circumpolar Current. *Rev. Geophys.,* **24,** 469–491.

Olbers, D., and M. Wenzel, 1989: Determining diffusivities from hydrographic data by inverse methods with applications to the circumpolar current. *Oceanic Circulation Models: Combining Data and Dynamics,* D. L. T. Anderson and J. Willebrand, Eds. Kluwer, 95–139.

Östlund, H. G., and M. Stuiver, 1980: GEOSECS Pacific radiocarbon. *Radiocarbon,* **22,** 25–53.

Rooth, C., 1982: Hydrology and ocean circulation. *Progress in Oceanography,* Vol. 11 Pergamon, 131–149.

Stommel, H., 1961: Thermohaline convection with two stable regimes of flow. *Tellus,* **13,** 224–230.

Walin, G., 1985: The thermohaline circulation and the control of ice ages. *Palaeogeogr., Palaeoclimatol., Palaeoecol.,* **50,** 323–332.

Warren, B. A., 1983: Why is no deep water formed in the North Pacific? *J. Mar. Res.,* **41,** 327–347.

Welander, P., 1986: Thermohaline effects in the ocean circulation and related simple models. *Large-Scale Transport Processes in Oceans and Atmosphere,* J. Willebrand and D. L. T. Anderson, Eds. D. Reidel, 163–200.

Whitworth, T., III, and R. G. Peterson, 1985: Volume transport of the Antarctic Circumpolar Current from bottom pressure measurements. *J. Phys. Oceanogr.,* **15,** 810–816.

Wolff, J. O., and D. J. Olbers, 1989: The dynamical balance of the Antarctic Circumpolar Current, studied with an eddy resolving quasigeostrophic model. *Mesoscale/Synoptic Coherent Structures in Geophysical Turbulence,* J. C. J. Nihoul and B. M. Jamart, Eds., Elsevier Science, 435–458.

Wunsch, C., 1984: An eclectic Atlantic Ocean circulation model. Part I: The meridional flux of heat. *J. Phys. Oceanogr.,* **14,** 1712–1733.